Powder Technology 367 (2020) 443–455

Contents lists available at ScienceDirect

Powder Technology

journal homepage: www.elsevier.com/locate/powtec

Numerical study on natural convection of Ag–MgO hybrid/water nanofluid inside a porous enclosure: A local thermal non-equilibrium model

S.A.M. Mehryan [a], Mohammad Ghalambaz [b,c,*], Ali J. Chamkha [d], Mohsen Izadi [e]

[a] Young Researchers and Elite Club, Yasooj Branch, Islamic Azad University, Yasooj, Iran
[b] Metamaterials for Mechanical, Biomechanical and Multiphysical Applications Research Group, Ton Duc Thang University, Ho Chi Minh City, Vietnam
[c] Faculty of Applied Sciences, Ton Duc Thang University, Ho Chi Minh City, Vietnam
[d] Mechanical Engineering Department, Prince Sultan Endowment for Energy and Environment, Prince Mohammad Bin Fahd University, Al-Khobar 31952, Saudi Arabia
[e] Mechanical Engineering Department, Faculty of Engineering, Lorestan University, Khorramabad, Iran

ARTICLE INFO

Article history:
Received 9 July 2019
Received in revised form 21 December 2019
Accepted 1 April 2020
Available online 3 April 2020

Keywords:
Hybrid nanofluids
LTNE model
Porous medium
Ag-MgO-water nanofluid
Natural convection

ABSTRACT

This paper investigates the natural convection of Ag-MgO/water nanofluids within a porous enclosure using a Local Thermal Non-Equilibrium (LTNE) model. The Darcy model is applied to simulate the flow dynamics throughout the porous medium. Using non-dimensional parameters, the dimensionless form of the prevailing equations has been derived. Finally, the Galerkin finite element method is utilized to solve governing equations using a non-uniform structured grid, numerically. The key parameters of this study are Rayleigh number ($10 \le Ra \le 1000$), porosity ($0.1 \le \varepsilon \le 0.9$), nanoparticles volume fraction ($0 \le \varphi \le 0.02$), interface convective heat transfer coefficient ($1 \le H \le 1000$), and the thermal conductivity ratio of two porous phases ($1 \le \gamma \le 10$). It is indicated that dispersing Ag–MgO hybrid nanoparticles in the water strongly decreases the transport of heat through two phases of the porous enclosure. For glass ball and aluminum foam, by increasing the H from 1 to 1000, Q_{hnf} would be 1.33 and 5.85 times, respectively, at $\varphi = 2\%$.

1. Introduction

The phenomenon of natural convection through porous materials has recently been an important topic owing to its wide applications, including solar collectors, building insulation, cooling of radioactive waste containers, nuclear engineering, fire control, energy systems storage, geothermal energy, and compact heat exchangers [1–8]. There are wide theoretical and practical studies dealing with natural convective inside enclosures [9–14].

Using nanofluid is a key strategy to achieve higher performance of thermal storage, solar collectors, heat exchangers, cooling of electronic ingredients, nuclear reactors. Commonly, nanofluids are produced by adding small nanoparticles of size between 1 and 100 nm. The thermal conductivity of such mixtures increases by applying the high thermal conductivity of metallic nanoparticles, which results in the total augmentation of energy transport through the thermal systems. Therefore, extensive research is being performed to apply nanofluids in situations where high heat flux should be rejected. Natural convection in cavities has its applications in engineering but has poor heat transfer performance when pure fluids are tested. Choi [15] reported improving the efficiency of various thermal systems using the nanofluids. However, several review investigations have been published updating developments in nanofluids [16–29]. Esfe et al. analyzed the thermal conductivity of CNTs-water [30], Al_2O_3 dispersed in ethylene glycol and water [31] as single nanofluid and SiO_2-MWCNT/ethylene glycol [32], ZnO-MWCNT/EG-water [33], SWCNT–Al_2O_3/ethylene glycol [34], CuO-SWCNTs-EG water [35] as hybrid nanofluid.

Ghasemi and Aminossadati [36] studied the natural convective inside an enclosure occupied with nanofluids with the contribution of Brownian motion and thermophoretic effects. Sun and Pop [37] investigated the flow and heat transfer of nanofluids in an enclosure. Aminossadati and Ghasemi [38] perused the enhanced natural convection inside an enclosure, which was saturated by a nanofluid. Chamkha and Abu-Nada [39] have perused the natural convection of water-based Al_2O_3 nanofluids for a different model of viscosity. Mahian et al. [40,41]

* Corresponding author at: Ton Duc Thang University, Ho Chi Minh City, Vietnam.
E-mail addresses: alal171366244@gmail.com (S.A.M. Mehryan), mohammad.ghalambaz@tdtu.edu.vn (M. Ghalambaz), achamkha@pmu.edu.sa (A.J. Chamkha), izadi.m@lu.ac.ir (M. Izadi).

https://doi.org/10.1016/j.powtec.2020.04.005
0032-5910/

performed an excellence review on the heat transfer mechanism of nanofluids.

Further study of nanofluids suggested a new class of nanofluids composed of different suspended nanoparticles called hybrid nanofluid. This is a slowly rising area of investigation, which is fabricated by dispersed a composite or mixture form of nanoparticles inside a host fluid. Using this class of nanofluids can cause the final price reduction, in addition to creating acceptable stability of nanofluids with high thermal conductivity; moreover, it provides the groundwork for massive industrialization. The goal of utilizing hybrid nanofluids is to further augment heat transfer by a comparison between features and drawbacks of single nanofluids, attributed to the stable aspect ratio, better thermal characteristics, and nanomaterials synergistic effect (see [42]).

In general, there are two methods for modeling heat transfer within a porous medium. The first model solves an energy equation in the porous medium by considering the Local Thermal Equilibrium (LTE) between the solid structure and fluid. Extensive studies have been carried out using this model on porous media [43–46]. The second model ignores the local thermal equilibrium between the solid structure and fluid. Therefore, the porous medium is modeled utilizing two separate energy equations for the solid and fluid to model the convective heat transfer. Some studies used LTNE model to simulate heat transfer through porous media are Alsabery et al. [47], Izadi et al. [48,49], Mehryan et al. [50,51], and Sivasankaran et al. [52]. Ghalambaz et al. [53] investigated the conjugate natural convection flow and heat transfer of hybrid nanofluids in a rectangular enclosure. The effect of the presence of a thermally conductive wall on the thermal behavior of the enclosure was investigated in the presence of Ag-MgO hybrid nanoparticles. The results showed that the presence of a conjugate wall significantly influences the practice of hybrid nanofluids in a porous medium. Although the study of Ghalambaz et al. [53] investigated the heat transfer of hybrid nanofluids in an enclosure, the results were not investigated for various types of porous mediums.

Taking note of the above-published works and following the study of Ghalambaz et al. [53], the present work aims to note the effectiveness of using hybrid nanofluids in various types of porous spaces, considering a two-temperature equation model. As a case study, and because the thermophysical data of nanofluid are available in the literature, it is accorded as a synthesized hybrid nanofluid. Does using a hybrid nanofluid improve the heat transfer? The glass balls porous matrix is considered as a low thermal conductive porous matrix, and the copper foam is also adopted as a porous matrix with high thermal conductivity. The applying of hybrid nanofluids in porous media is new, and it has not been analyzed yet. Base on "What advantages does the using hybrid nanofluid have over regular nanofluids?" and "How do LTNE model and the phase interaction affect the effectiveness of exerting hybrid nanofluids as heat transfer agents?", the present study aims to address the effect of using hybrid nanofluids in porous media by considering local thermal non-equilibrium effects for the first time.

We now progress to the next section to formulate the natural convective of Ag–MgO/Water nanofluids in a porous-filled enclosure.

2. Basic equations

2.1. Governing equtions

In Fig. 1, a simple schematic view of the nanofluid-saturated porous enclosure with a size of L has been shown. Ag-MgO/ water hybrid nanofluid occupies the void spaces of the medium. The horizontal bounds of the cavity have been fully insulated, whereas, the left and right of the enclosure have the high and low temperatures of T_h^* and T_c^* so that $T_h^* > T_c^*$. The hybrid nanoparticles have continuously been suspended with the help of surface charge technology or surfactant. The use of these strategies does not allow hybrid nanoparticles to be deposited and/or agglomerated. A homogeneous and isotropic structure is considered for the porous medium. The convicting nanofluid and the solid matrix are not thermally equilibrated.

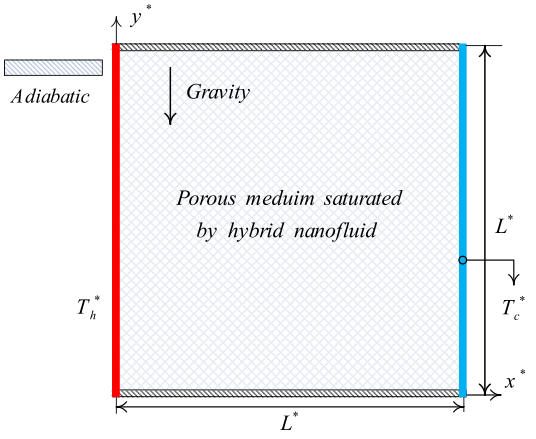

Fig. 1. A simple view of the geometry of the physical model.

The suspension is considered to be Newtonian and viscous. Besides, flow arising from natural convection is laminar. No thermal and dynamic slips are found between the suspended hybrid nanoparticles and the host fluid. It is assumed that the surface of the porous matrix is treated to avoid filtration of nanoparticles. Although the flow is incompressible, the convection is attributed to the variations of the density modeled by the Boussinesq approximation. The usage of Darcy law to tracking dynamic behavior of the suspension and applying the assumptions lead to the following equations (Nield and Bejan [4]):

$$\frac{\partial u^*_{hnf}}{\partial x^*}+\frac{\partial v^*_{hnf}}{\partial y^*}=0 \tag{1}$$

$$0=-\frac{\partial p^*}{\partial x^*}-\frac{\mu_{hnf}}{K}u^*_{hnf} \tag{2}$$

$$0=-\frac{\partial p^*}{\partial y^*}-\frac{\mu_{hnf}}{K}v^*_{hnf}-(\rho\beta)_{hnf}\left(T^*_{hnf}-T^*_c\right)g \tag{3}$$

$$(\rho C_p)_{hnf}\left(u^*_{hnf}\frac{\partial T^*_{hnf}}{\partial x^*}+v_{hnf}\frac{\partial T^*_{hnf}}{\partial y^*}\right)=\varepsilon k_{hnf}\left(\frac{\partial^2 T^*_{hnf}}{\partial x^{*2}}+\frac{\partial^2 T^*_{hnf}}{\partial y^{*2}}\right)+h\left(T^*_s-T^*_{hnf}\right) \tag{4}$$

$$0=(1-\varepsilon)k_s\left(\frac{\partial^2 T^*_s}{\partial x^{*2}}+\frac{\partial^2 T^*_s}{\partial y^{*2}}\right)+h\left(T^*_{hnf}-T^*_s\right) \tag{5}$$

where u^*_{hnf} and v^*_{hnf} are the components of the Darcian velocity vector. k, K, p, T^* and g represent the thermal conductivity, permeability, pressure, temperature, and gravitational acceleration, respectively. β, μ, C_p, and ρ indicate the coefficient of the thermal expansion, dynamic viscosity, specific heat at constant pressure, and density, respectively. The ε is the porosity and h is the heat transfer coefficient of the interface convective.

Table 1
Thermal conductivity and dynamic viscosity of the suspension [54].

φ_{hnp} (%)	k_{hnf}/k_{bf}	μ_{hnf}/μ_{bf}	M	α_r
0	1	1	1	1
0.56	1.05376	1.063619	0.93789	1.0555
1.12	1.08296	1.160534	0.85746	1.0866
1.5	1.13208	1.300207	0.76407	1.1371
2	1.1573	1.3815	0.71753	1.1642

Table 2
The relations describing the thermo-physical properties [55].

Thermo-physical property	Relation
Density	$\rho_{hnf}=\rho_f(1-\varphi_{hnp})+\rho_{Ag}\varphi_{Ag}+\rho_{MgO}\varphi_{MgO}$
heat capacity	$(\rho C_p)_{hnf}=(1-\varphi_{hnp})(\rho C_p)_{bf}+\varphi_{Ag}(\rho C_p)_{Ag}+\varphi_{MgO}(\rho C_p)_{MgO}$
buoyancy coefficient	$(\rho\beta)_{hnf}=(1-\varphi_{hnp})(\rho\beta)_{bf}+\varphi_{Ag}(\rho\beta)_{Ag}+\varphi_{MgO}(\rho\beta)_{MgO}$
Thermal diffusivity	$\alpha_{hnf}=k_{hnf}/(\rho C_p)_{hnf}$

Utilizing the experimental data, Table 1 represents thermal conductivity and dynamic viscosity of Ag-MgO hybrid/water nanofluid for different values of the nanoparticles concentration [54]. In this table, two dimensionless parameters M and α_r are functions of the total volume fraction and will be explained later. The relations summarized in Table 2 along with data of Table 3 are used to obtain the values of other thermophysical properties.

The relations represented in [54], obtained by curve-fitting on the experimental data, have been listed below.

$$k_{hnf}=\left(\frac{0.1747\times10^5+\varphi_{hnp}}{0.1747\times10^5-0.1498\times10^6\varphi_{hnp}+0.1117\times10^7\varphi_{hnp}^2+0.1997\times10^8\varphi_{hnp}^3}\right)k_{bf}$$
$$0\le\varphi_{hnp}\le0.03 \tag{6}$$

$$\mu_{hnf}=\left(1+32.795\varphi_{hnp}-7214\varphi_{hnp}^2+714600\varphi_{hnp}^3-0.1941\times10^8\varphi_{hnp}^4\right)\mu_{bf} \tag{7}$$
$$0\le\varphi_{hnp}\le0.02$$

Using the cross-differentiating between the Eqs. (2) and (3), the pressure can be eliminated. Hence, the continuity and the momentum equations are rewritten as:

$$\frac{\partial u_{hnf}^*}{\partial x^*}+\frac{\partial v_{hnf}^*}{\partial y^*}=0 \tag{8}$$

$$\frac{\mu_{hnf}}{K}\left(\frac{\partial u_{hnf}^*}{\partial y^*}-\frac{\partial v_{hnf}^*}{\partial x^*}\right)=-g(\rho\beta)_{hnf}\frac{\partial T_{hnf}^*}{\partial x^*} \tag{9}$$

Two above equations can be merged using a new variable, namely stream function so that $u_{hnf}^*=\frac{\partial\psi^*}{\partial y}$, $v_{hnf}^*=-\frac{\partial\psi^*}{\partial x}$. The following variables now are presented:

$$x=\frac{x^*}{L^*},y=\frac{x^*}{L^*},\psi=\frac{\psi^*}{\alpha_{bf}},T_{hnf}=\frac{\left(T_{hnf}^*-T_c^*\right)}{\left(T_h^*-T_c^*\right)},T_s=\frac{\left(T_s^*-T_c^*\right)}{\left(T_h^*-T_c^*\right)} \tag{10}$$

The equations are rewritten in a non-dimensionless way by applying the above variables:

$$\frac{\partial^2\psi}{\partial x^2}+\frac{\partial^2\psi}{\partial y^2}=-Ra.M.\frac{\partial T_{hnf}}{\partial x} \tag{11}$$

Table 3
The thermophysical properties of nanofluid components [37,55].

Properties	MgO	Ag	Water
C_p (J/kg. K)	955	235	4179
k (W/m. K)	45	429	0.613
ρ (kg/m^3)	3560	10,500	997.1
$\beta\times10^{-5}$ (K^{-1})	1.05	1.89	21
$\mu\times10^{-4}$ (kg/m. s)	–	–	8.9
$\alpha\times10^{-7}$ (m^2/s)	–	1738.6	1.47

Where

$$Ra=\frac{gK\rho_{bf}\beta_{bf}\left(T_h^*-T_c^*\right)L}{\alpha_{bf}\mu_{bf}},M=\left(\frac{(\rho\beta)_{hnf}}{(\rho\beta)_{bf}}\right)\left(\frac{\mu_{bf}}{\mu_{hnf}}\right) \tag{12}$$

$$\frac{1}{\varepsilon}\left(\frac{\partial\psi}{\partial y}\frac{\partial T_{hnf}}{\partial x}-\frac{\partial\psi}{\partial x}\frac{\partial T_{hnf}}{\partial y}\right)=\alpha_r\left(\frac{\partial^2T_{hnf}}{\partial x^2}+\frac{\partial^2T_{hnf}}{\partial y^2}\right)+\frac{(\rho C_p)_{bf}}{(\rho C_p)_{hnf}}H\left(T_s-T_{hnf}\right) \tag{13}$$

$$0=\left(\frac{\partial^2T_s}{\partial x^2}+\frac{\partial^2T_s}{\partial y^2}\right)+\gamma H\left(T_{hnf}-T_s\right) \tag{14}$$

where

$$H=\frac{hL^2}{\varepsilon k_{bf}},\gamma=\frac{\varepsilon k_{bf}}{(1-\varepsilon)k_s},\alpha_r=\frac{\alpha_{hnf}}{\alpha_{bf}} \tag{15}$$

H and γ of the above-written relation are respectively, the interface heat transfer coefficient and modified thermal conductivity ratio. Indeed, γ denotes the porosity-scaled thermal conductivity ratio for the porous medium. It should be noted that the Darcy model is adopted in the present study, and the Rayleigh number, in Eq. (12), denotes the Darcy-Rayleigh number. Hence, it is not the same as the regular Rayleigh number in a clear flow of the Darcy-Brinkman model. The mathematical forms of the boundary conditions are presented below:

$$\begin{aligned}
&\psi=0,\quad T_s=T_{hnf}=1 \quad at \quad x=0\\
&\psi=0,\quad T_s=T_{hnf}=0 \quad at \quad x=1\\
&\psi=0,\quad \frac{\partial T_s}{\partial y}=\frac{\partial T_{hnf}}{\partial y}=0 \quad at \quad y=0\\
&\psi=0,\quad \frac{\partial T_s}{\partial y}=\frac{\partial T_{hnf}}{\partial y}=0 \quad at \quad y=1
\end{aligned} \tag{16}$$

2.2. Heat transfer rates

The rate of transferred heat through the fluid and solid components of the porous medium are determined by using the following relations:

$$Nu_{hnf}=\frac{1}{L}\int_0^L\left(\frac{\partial T_{hnf}}{\partial x}\right)dy \tag{17}$$

$$Nu_s=\frac{1}{L}\int_0^L\left(\frac{\partial T_s}{\partial x}\right)dy \tag{18}$$

where $Nu_{hnf}=h.L/k_{hnf}$. The combination of two above relations gives the total heat transfer, i.e., Q_{hnf}:

$$Q_{hnf}=\varepsilon k_{hnf}\int_0^L\left(\frac{\partial T_{hnf}}{\partial x}\right)dy+k_s(1-\varepsilon)\int_0^L\left(\frac{\partial T_s}{\partial x}\right)dy \tag{19}$$

Finally, Q_r, the ratio of the total heat transfer rate of nanofluid to the pure fluid is:

$$Q_r=\frac{Q_{hnf}}{Q_{hnf}|_{\varphi=0}}=\frac{\varepsilon\frac{k_{hnf}}{k_s}Nu_{hnf}+(1-\varepsilon)Nu_s}{\left(\varepsilon\frac{k_{hnf}}{k_s}Nu_{hnf}+(1-\varepsilon)Nu_s\right)_{\varphi=0}} \tag{20}$$

It should be noted that there are two channels of heat transfer from the surface. The heat can go through the solid matrix and enter the cavity, or it can go through the liquid and enter the cavity. The Nusselt

Table 4
Grid study; $Ra = 10^3$, $H = 100$, $\gamma = 10$, $\varepsilon = 0.9$ and $\varphi = 0.0$.

Case number (i)	Grid size	Nu_{hnf}	*Error* (%)	Nu_s	*Error* (%)	$\lvert\psi\rvert_{max}$	*Error* (%)
1	50 × 50	14.200	–	6.958	–	20.219	–
2	100 × 100	14.188	0.084	6.973	0.216	20.170	0.242
3	150 × 150	14.185	0.021	6.975	0.028	20.161	0.045
4	200 × 200	14.185	0.000	6.976	0.014	20.158	0.015

numbers in solid and liquid phases denote the non-dimensional heat transfer rate for each of these two possible channels. Here, Q_r shows the overall heat transfer through both solid and liquid channels. Q_r displays the enhancement or reduction of the total heat transfer rate due to dispersing the hybrid nanoparticles in the host fluid. The solid matrix of the porous medium can be glass balls ($k_s = 1.05$ W.m^{-1} K^{-1}) or aluminum foam ($k_s = 205$ W.m^{-1} K^{-1}).

3. Numerical methodology

To solve the partial differential three-equation set and the boundary conditions given in Eq. (14) the Galerkin finite element method is exerted. First, the partial equations are presented in equivalent weak forms. To investigate the residuals, the bi-quadratic functions along with the three-point Gaussian quadrature are used. Moreover, the residual equations are solved by applying the Newton–Raphson iterative approach. A detailed discretization of the equations and the numerical methodology was completely described in [56].

The outcomes of the simulation need to be independent of the number of elements discretizing the computational domain. Hence, the grid study is performed before validating. A non-uniform structured grid with quadratic elements is applied to discretizing the domain to subdomains. As indicated in Table 4, the results indicate a negligible difference between the 100 × 100 and 150 × 150. Therefore, the grid size of 100 × 100 is confidently utilized in all calculations. It is worth mentioning that the Errors (**%**) in this table are calculated as follows:

$$Error\ (\%) = \frac{|\delta_{i+1} - \delta_i|}{|\delta_i|} \times 100 \tag{21}$$

Where δ_i can be Nu_{hnf}, Nu_s or $|\psi|_{max}$. i index also denotes to the grid case number as depicted in Table 4.

Comparing the current outcomes and those reported in the literature, the validity of the utilized code is evaluated [37,57,58]. The values reported in Table 5 belong to a porous triangular-shaped enclosure containing Cu-water nano-fluid. In the other validation, the heat transfer rates through a porous medium of the current solution and Baytas and pop' solution [58] are compared(depicted in Fig. 2). In both validations, an excellent agreement exists between the present results and the results of the published studies. Hence, to use the current code, a strong certainty exists.

4. Results and discussion

In this portion, the consequences of the numerical solution of Eqs. (11)–(13) subject to the boundary conditions (14) are given and discussed for the streamlines, isotherms of fluid and solid phases, and the heat transfer rates. To represent the consequences, the key parameters vary in these ranges; Rayleigh number: $10 \le Ra \le 1000$, porosity: $0.1 \le \varepsilon \le 0.9$, the volume fraction of the nanoparticles: $0 \le \varphi \le 0.02$, interface heat transfer coefficient: $1 \le H \le 1000$ and modified thermal conductivity ratio: $0.1 \le \gamma \le 10$. At the end of the section, the impacts of Ag, MgO, and Ag-MgO nanoparticles on the heat transfer rates will be compared with each other.

In Fig. 3, the influences of *Ra* on the flow patterns and the isotherms of the fluid and solid phases are presented. An increment in *Ra*, which means the augmentation of the buoyancy force, leads to amplification of the flow strength. The negative values of the streamlines display the anti-clockwise rotations of the vortices. In fact, the temperature gradient of the left hot bound and the adjacent cold fluid creates a lifting force. In contrast, a lowering force is created as a result of the temperature difference of the right cold bound and the adjacent hybrid nanofluid. In these patterns, the solid and dashed lines are related to the pure fluid and hybrid nanofluid with $\varphi = 0.02$. The increase in buoyancy force also occasions that the circular-shaped streamlines are horizontally stretched. Also, it is concluded that the existence of suspended hybrid nanoparticles declines the flow strength. Indeed, the resistance of the fluid against the buoyancy forces is augmented as a result of the larger dynamic viscosity of the Ag-MgO hybrid nanofluid.

It is evident that the isotherms of the fluid phase are almost parallel to the vertical boundaries. The distortions of isotherms increase as *Ra* boosts so that the isothermal is stratified when $Ra = 1000$. These horizontal classifications indicate the convection is the principal mechanism for the heat transfer. Moreover, at the low value of the Rayleigh number (i.e., $Ra = 10$), the temperature in the solid and fluid phases are near to each other. As Rayleigh number increase, the difference between the temperature fields of the fluid and solid phases is more obvious. At low *Ra* values (i.e. $Ra = 10$ and 100), the conduction is the principal mechanism of heat transfer, the influences of Ag-MgO hybrid nanoparticles on the thermal field of the solid phase are partly visible. While, when $Ra = 1000$, the thermal field of the solid phases is not influenced by the Ag-MgO hybrid nanoparticles. Moreover, the usage of the Ag-

Table 5
The average Nusselt number for the present work and others [37,57].

Ra	φ	Sheremet et al. [57]	Sun and Pop [37]	Present work
500	0	9.65	9.66	9.64
1000	0.1	9.41	9.42	9.42
500	0	14.05	13.9	13.96
1000	0.2	12.84	12.85	12.85

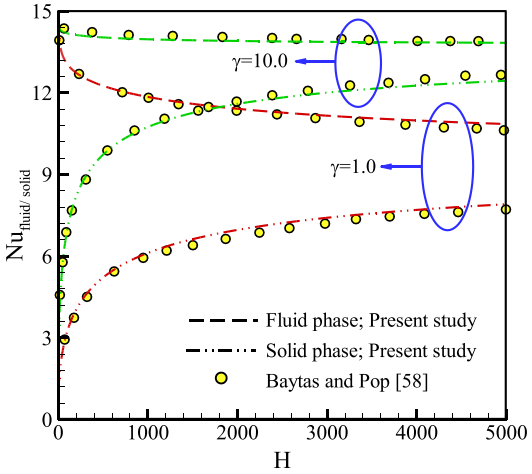

Fig. 2. the results of present work and represented in [58].

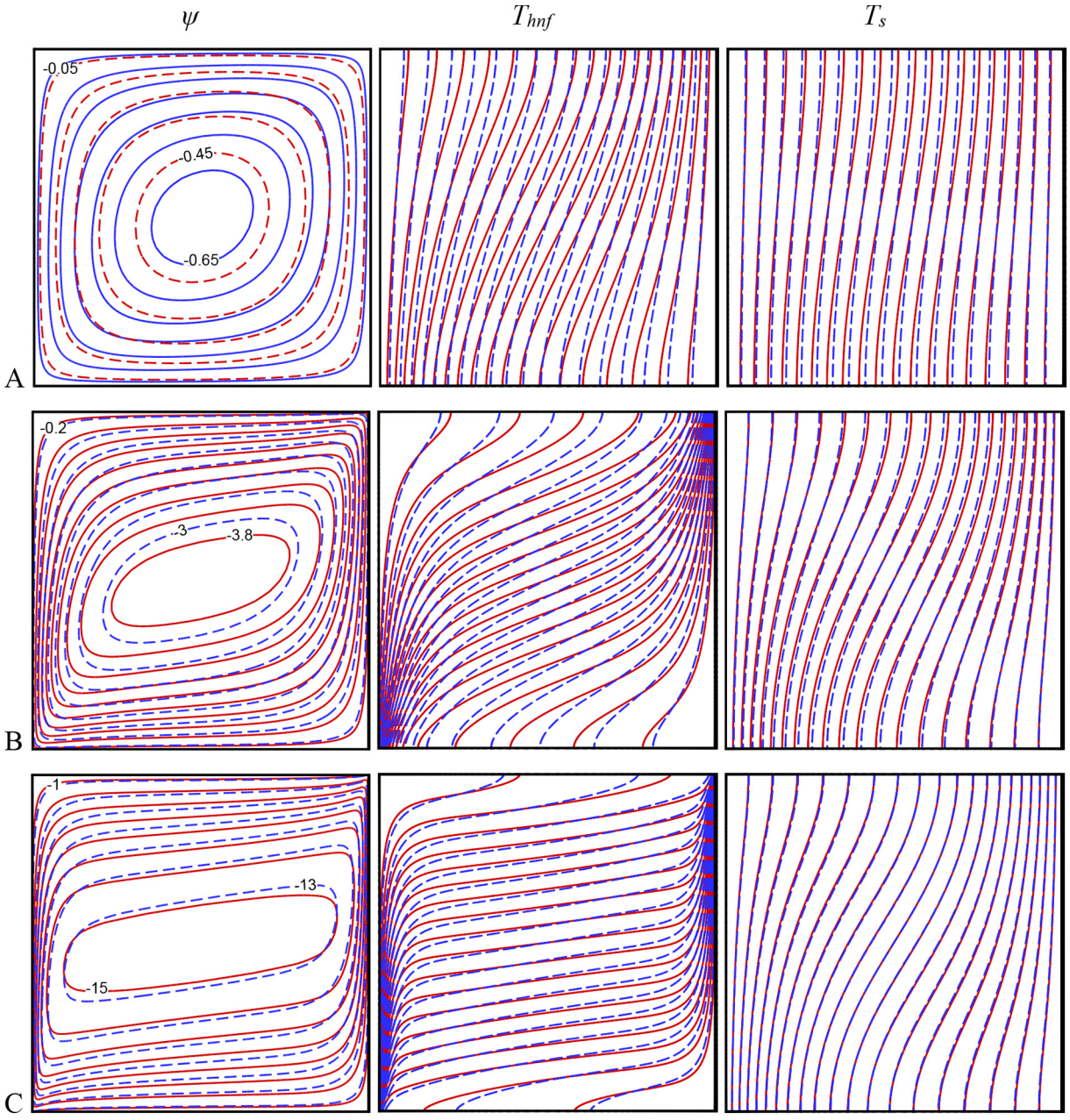

Fig. 3. Independency of the flow patterns and temperature fields of the pure fluid (solid lines) and hybrid nanofluid (dash lines) on *Ra*; A: $Ra = 10$, B: $Ra = 100$, C: $Ra = 1000$, $\varepsilon = 0.5$, $H = 10$ and $\gamma = 1$.

MgO hybrid nanoparticles declines the local thermal non-equilibrium condition between two phases of the porous medium. This result is clearly observed for $Ra = 1000$.

The independence of the flow patterns and the temperature fields of the fluid and solid phases on the modified thermal conductivity ratio γ is presented in Fig. 4. When γ increases, the strength of the recirculation in the porous medium slightly declines. The low value of γ implies that the fluid phase thermal conductivity is low compared to the solid phase. Therefore, most of the heat is transferred through the solid phase.

In low values of γ, the solid phase isotherms are parallel to the vertical bounds, and an increment in γ causes the distortions of the isotherms to increase. Indeed, when γ is low, a drastic local thermal non-equilibrium effects are observed between the fluid and solid phases and this non-equilibrium state gradually approaches the thermal equilibrium state by increasing the γ. It is can be seen that dispersing the Ag-MgO hybrid nanoparticles causes the elongation of the fluid phase isotherms to decrease. On the other hand, the location of the solid phase isotherms remains fixed. Hence, it is concluded that the usage of the Ag-MgO hybrid nanoparticles directs the isotherms of the two phases to a unit isotherm.

The independence of the flow patterns and temperature fields of the fluid and solid phases on the interface heat transfer parameter H is demonstrated in Fig. 5. The size and power of the recirculation increase with an augmentation of H. The interface parameter H is a test of the heat transfer rate microscopically between the solid and fluid phases. Therefore, the augmentation of H leads to more significant heat transfer between these two phases. Consequently, the thermal boundary layer thickness increases with H. Additionally, increasing the H causes the solid phase isotherms to become more stretched. Indeed, the increase in the H conducts both temperature fields to a unique one. It is apparent

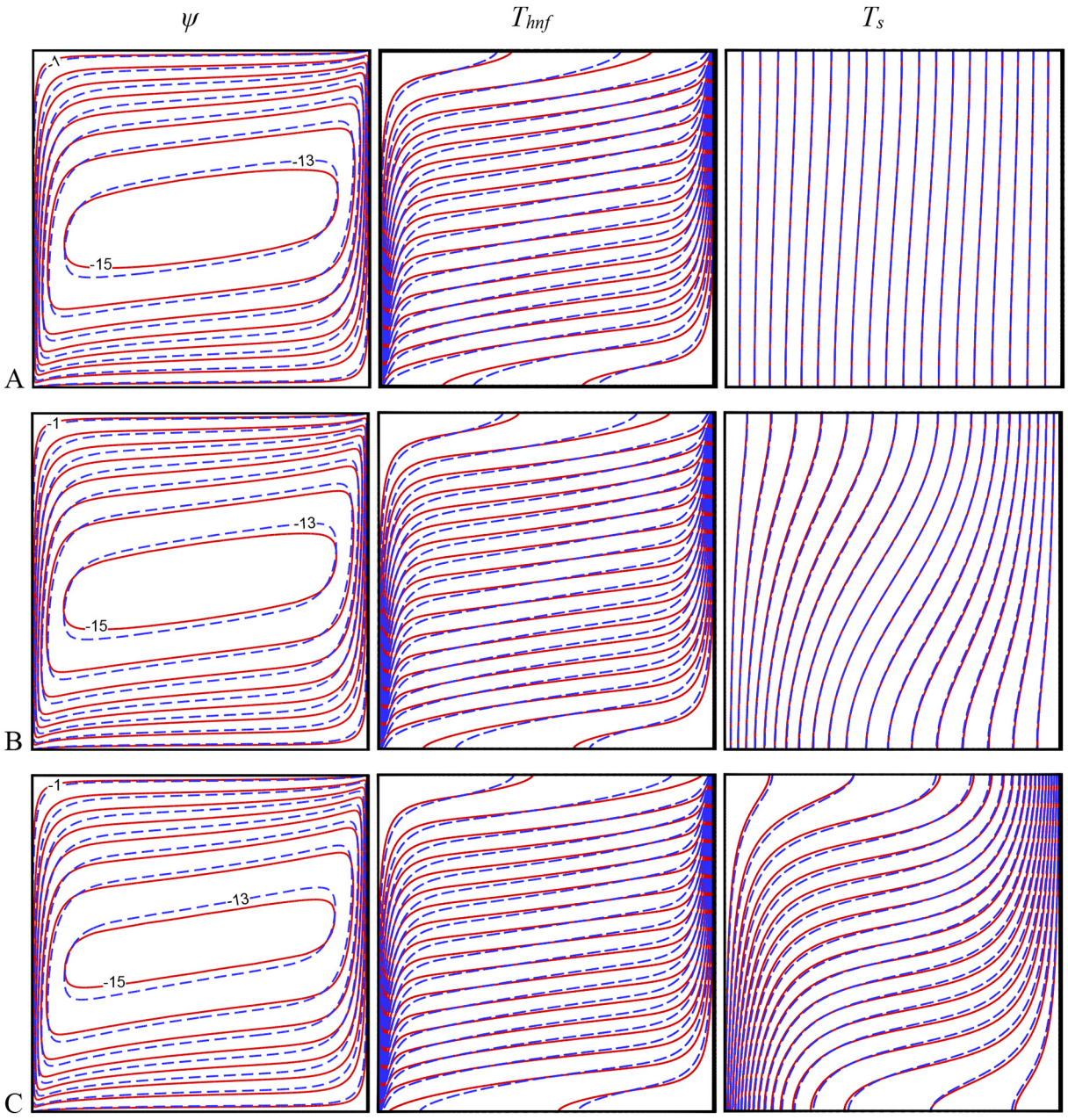

Fig. 4. Independency of the flow patterns and temperature fields of the pure fluid (solid lines) and hybrid nanofluid (dash lines) on γ; A: $\gamma = 0.1$, B: $\gamma = 1.0$, C: $\gamma = 10$, $Ra = 1000$, $\varepsilon = 0.5$, $H = 10$.

that the presence of hybrid nanoparticles significantly affects the solid phase temperature field at high values of H (i.e., $H = 100$ and 1000).

As depicted in Fig. 6, an increment in porosity causes the strength and recirculation size created inside the porous cavity to enhance. Indeed, when porosity enhances, the hybrid nanofluid motion becomes more convenient in the cavity. It is understood that the horizontal stretch of the fluid phase isotherms diminishes while increasing ε. However, the solid phase temperature field is insignificantly influenced by the increment of the ε.

The data presented in Table 6 indicate that growth in the Ra enhances the heat transfer rates through the fluid and solid phases. Moreover, it is concluded that the nanofluid flow strength is strongly amplified by increasing Ra. Additionally, the usage of the hybrid nanoparticles reduces the heat transfer rates and fluid flow strength. The decrease of Nu_{hnf} because of applying the hybrid nanoparticles is more when Ra is higher.

Fig. 7 depicts the dependency of the heat transfer rates on the H and γ for both hybrid nanofluid and pure fluid. The increment of the H leads to a decline in Nu_{hnf}. the thermal boundary layer thickens with growing the H, resulting in the reduction of Nu_{hnf}. It can visibly be observed that the decreasing effects of H on the Nu_{hnf} diminish with increasing γ. In fact, the temperature fields of the solid and fluid phases are directed in a unified field as γ is heightened.

As mentioned, γ is the thermal resistance ratio of the solid phase to the fluid phase. When γ is high, i.e., $\varepsilon k_{bf} \geq (1-\varepsilon)k_s$, the thermal conductivity of the fluid phase is significant. In such a case, most of the heat will be carried out by the fluid convection and partly by conduction through the solid phase. In fact, at the high values of γ the temperature fields of

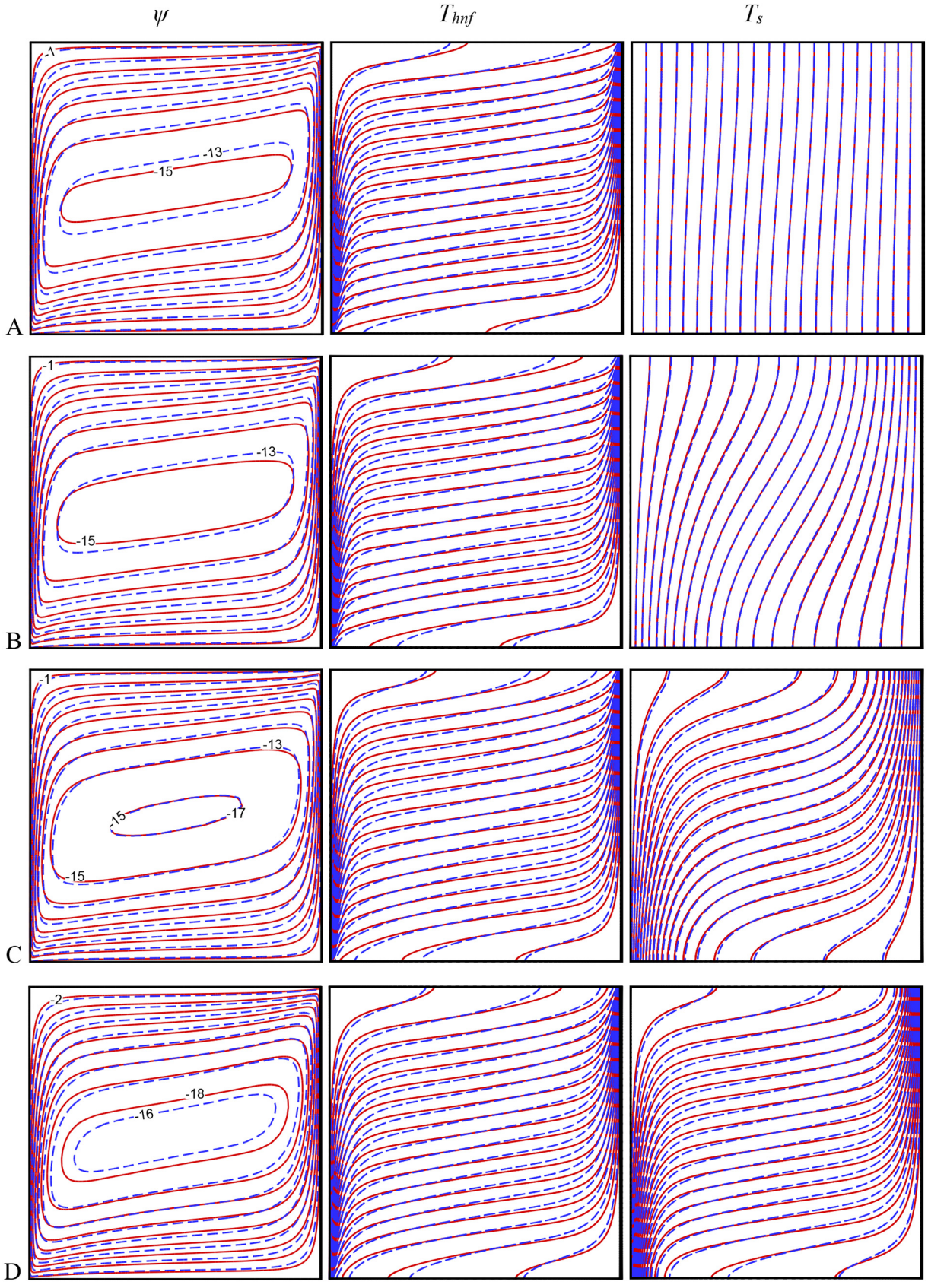

Fig. 5. Independency of the flow patterns and temperature fields of the pure fluid (solid lines) and hybrid nanofluid (dash lines) on the H; A: $H = 1$, B: $H = 10$, C: $H = 100$, D: $H = 1000$, $Ra = 1000$, $\varepsilon = 0.5$ and $\gamma = 1$.

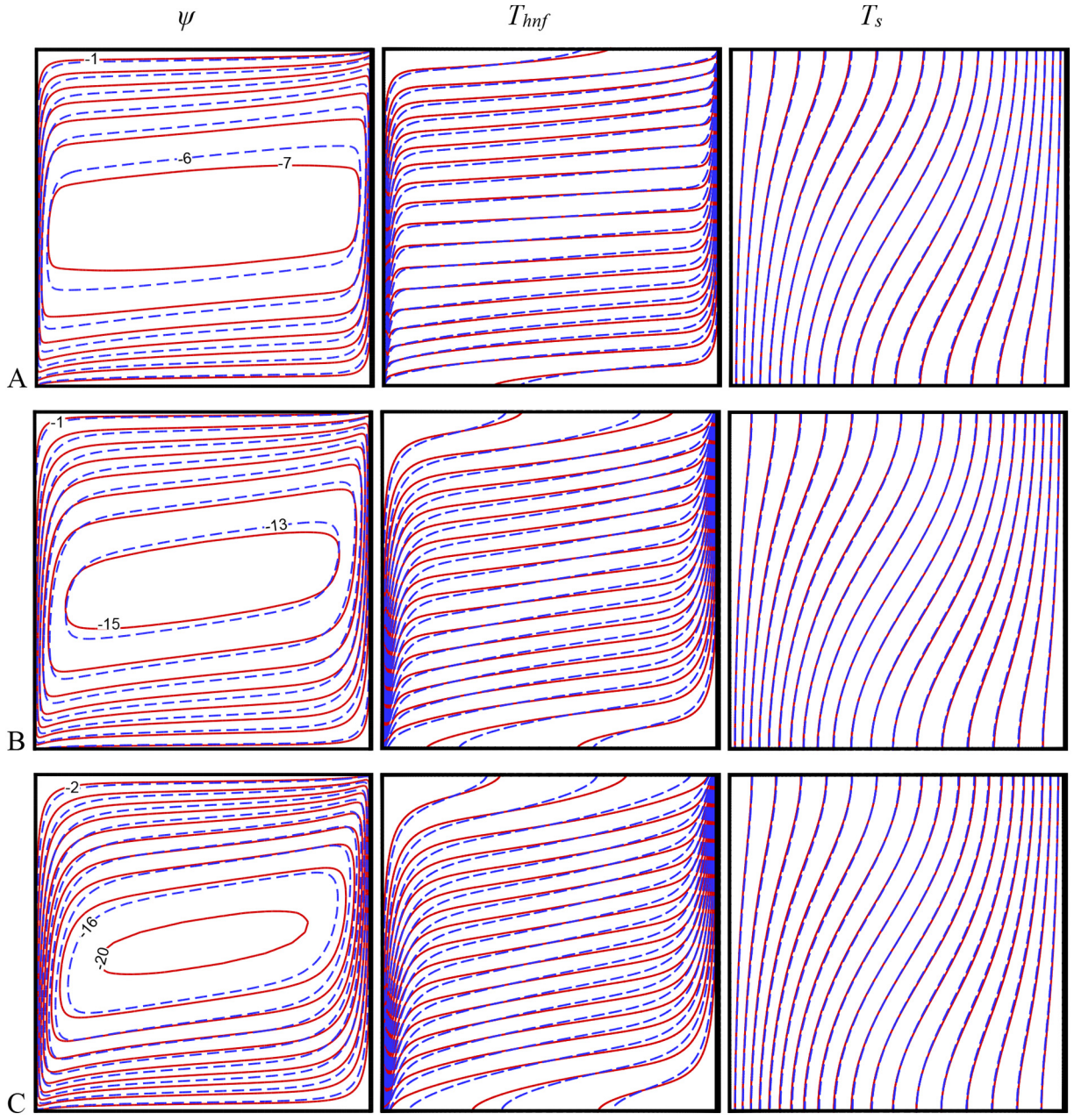

Fig. 6. Independency of the flow patterns and temperature fields of the pure fluid (solid lines) and hybrid nanofluid (dash lines) on the ε; A: $\varepsilon = 0.1$, B: $\varepsilon = 0.5$, C: $\varepsilon = 0.9$, $Ra = 1000$, $H = 10$ and $\gamma = 1$.

Table 6
Dependency of the heat transfer rates on the Ra and φ at $\varepsilon = 0.5$, $H = 10$ and $\gamma = 1$.

Ra	φ (%)	Nu_{hnf}	Nu_s	$\lvert\psi\rvert_{max}$
10	0.0	1.1848	1.0323	0.69690
	1.12	1.1245	1.0223	0.60801
	2	1.0814	1.0150	0.51550
100	0.0	4.5784	1.2950	4.0194
	1.12	3.8962	1.2654	3.7198
	2	3.2865	1.2335	3.3604
1000	0.0	19.779	1.5313	15.710
	1.12	17.280	1.5140	14.947
	2	14.970	1.4945	13.918

solid and fluid phases are locally near to each other. Hence, the heat transfer rate is low between these two phases. On the other hand, as presented in Fig. 7 (b), it can be determined that Nu_s increase when H grows. Moreover, it is obvious that the variations of Nu_{hnf} and Nu_s are insignificant when the H parameter is higher than 50×10^3. In fact, for the high values of the H parameter, the fluid and solid phases of the porous medium have locally the same temperature, resulting in the local thermal equilibrium condition.

Fig. 8 demonstrates the dependency of the Nu_{hnf} and Nu_s on the nanoparticles volume fraction at the various values of ε. An increment in the hybrid nanoparticle concentration reduces the heat transfer

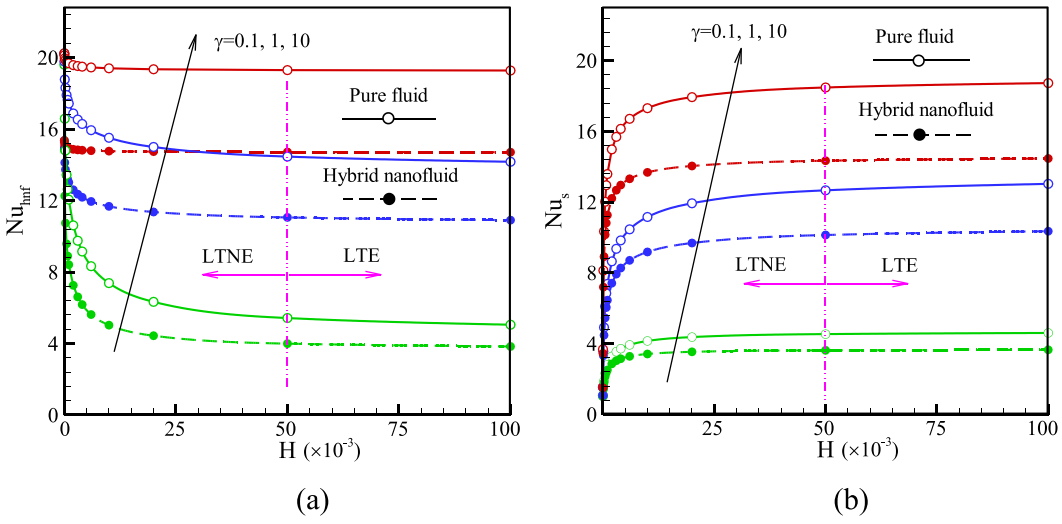

Fig. 7. The dependency of (a): Nu_{hnf} and (b): Nu_s on the H and γ for pure fluid and hybrid nanofluid when $Ra = 1000$, $\varphi = 0.02$ and $\varepsilon = 0.5$.

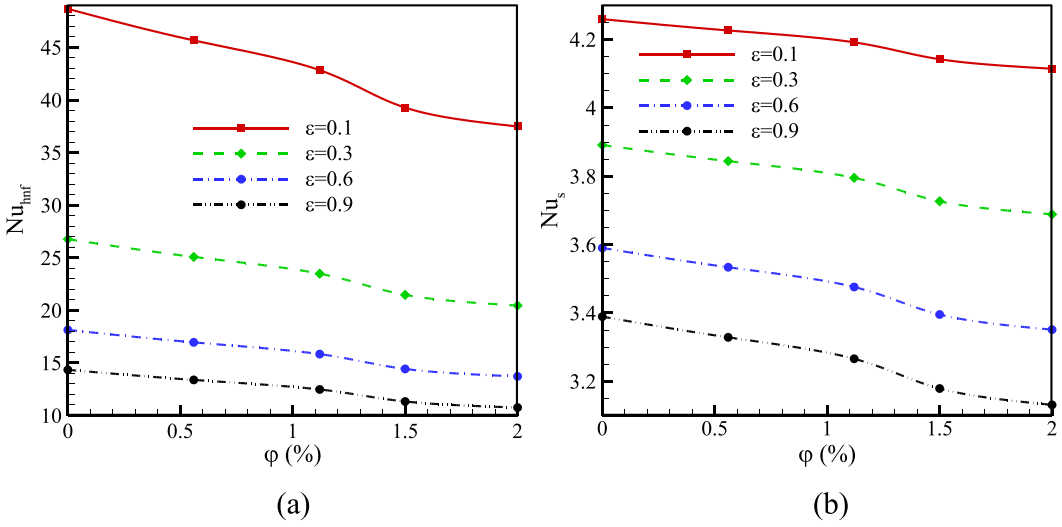

Fig. 8. Dependency of (a): Nu_{hnf} and (b): Nu_s on the φ and ε when $Ra = 1000$ and $H = \gamma = 10$.

rates for all the values of ε. As shown in Fig. 8 (a), the reduction of Nu_{hnf} with increasing φ is less when ε is higher. From Fig. 8 (b), a reverse trend can be seen for the solid phase. Moreover, as presented in Fig. 8, an increase in the ε diminishes the rates of heat transfer.

The data given in Table 7 presents the total heat transfer rate, Q_{hnf}, for different values of φ and ε for the solid matrices of glass balls and aluminum foam. The results illustrate that when the solid matrix is glass balls, an increase in ε leads to an increment in the Q_{hnf}. While increasing ε of the porous medium with aluminum foam reduces Q_{hnf}.

Table 7
dependency of Q_{hnf} on the φ and ε for the porous medium with solid matrices of glass balls and aluminum foam; $Ra = 1000$, $H = 10$ and $\gamma = 1$.

φ (%)	Glass balls			Aluminum foam		
	$\varepsilon = 0.1$	$\varepsilon = 0.5$	$\varepsilon = 0.9$	$\varepsilon = 0.1$	$\varepsilon = 0.5$	$\varepsilon = 0.9$
0	4.493685	6.86616	7.8834	301.8625	163.016	38.15255
0.56	4.45578	6.7746	7.75152	300.9605	162.073	37.8184
1.12	4.344795	6.52827	7.424235	299.9355	160.9086	37.2731
1.5	4.21974	6.25002	7.047705	298.521	159.3547	36.59455
2	4.14939	6.093675	6.83739	297.701	158.4855	36.2153

The total heat transfer rate, Q_{hnf}, for different values of H is given in Table 8 for both materials of the solid matrix. The obtained results indicate that the Q_{hnf} amplifies with increasing the H. As previously shown, increasing the H results in a decrease and increase in the heat transfer rates through the fluid and solid phase, respectively. Since the reduction of heat transfer of the fluid phase is less compared to the augmentation of heat transfer of the other phase, Q_{hnf} enhances with boosting H.

In order to carry out a more detailed study, the independence of the total heat transfer ratio Q_r on the hybrid nanoparticles concentration φ is studied as Ra, H, ε, and γ vary (Figs. 9-12). As observed in Fig. 9, excluding $Ra = 10$ for the glass balls, the Q_r decreases with growing the nanoparticles volume fraction φ. As the experimental data show, dispersing the hybrid nanoparticles inside the host fluid increases the thermal conductivity and dynamic viscosity, which these phenomena lead to the increase and decrease in the heat transfer rate, respectively. For the solid matrix of glass balls, dispersing the hybrid nanoparticles with $\varphi = 0.56\%$ decreases the Nusselt number at $Ra = 10$. In fact, the heat transfer reduction by the increase in dynamic viscosity is dominant

Table 8
dependency of Q_{hnf} on the φ and H for the porous medium with solid matrices of glass balls and aluminum foam; $Ra = 1000$, $\varepsilon = 0.5$ and $\gamma = 1$.

φ (%)	Glass balls				Aluminum foam			
	$H = 1$	$H = 10$	$H = 100$	$H = 1000$	$H = 1$	$H = 10$	$H = 100$	$H = 1000$
0	6.75528	6.86511	7.61964	9.21186	115.0706	163.0058	370.1275	761.124
0.56	6.667395	6.773865	7.504875	9.016875	114.8923	162.0628	364.4285	739.2095
1.12	6.42705	6.530055	7.236495	8.663235	114.5561	160.9127	358.0735	715.163
1.5	6.153	6.250965	6.923385	8.2383	114.144	159.3588	349.402	683.183
2	6.01965	6.11499	6.770295	8.03061	113.9411	158.5655	344.9945	667.2955

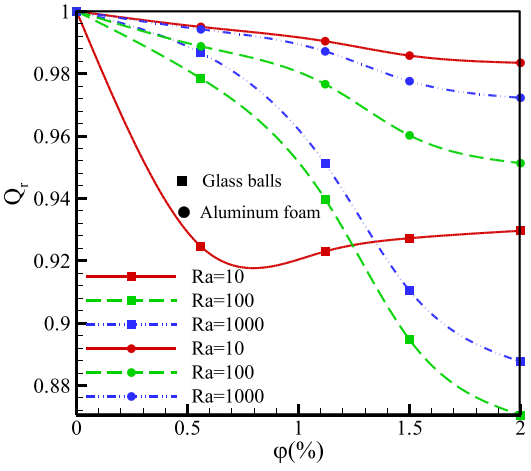

Fig. 9. Dependency of the Q_r on the φ when Ra varies; $H = 10$, $\gamma = 1$ and $\varepsilon = 0.5$.

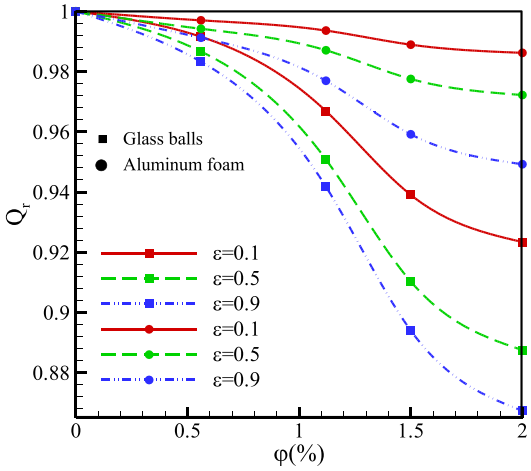

Fig. 11. Dependency of the Q_r on the φ when ε varies; $Ra = 1000$, $H = 10$ and $\gamma = 1$.

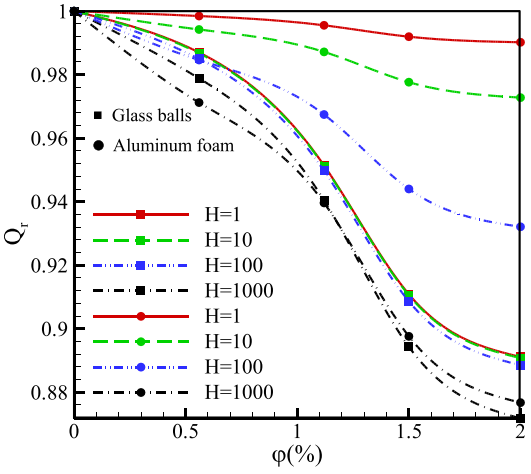

Fig. 10. Dependency of the Q_r on φ when H varies; $Ra = 1000$, $\gamma = 1$ and $\varepsilon = 0.5$.

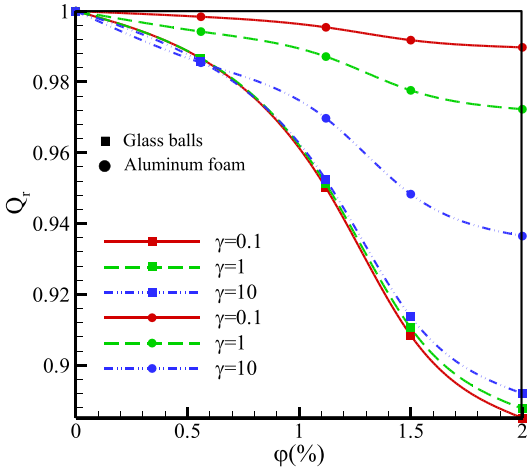

Fig. 12. The dependency of the Q_r on φ when γ varies; $Ra = 1000$, $H = 10$ and $\varepsilon = 0.5$.

compared with its increment by the thermal conductivity. On the other hand, this trend is reversed when the volume fraction is $\varphi > 0.56$.

It may also be observed that the maximum reduction of Q_{hnf} due to the presence of the Ag–MgO hybrid nanoparticles occurs at $Ra = 100$. Fig. 10 demonstrates that the reduction value of Q_{hnf}, as a result of dispersing Ag–MgO hybrid nanoparticles, is more when the H is higher. Generally, this reduction for glass balls is much more than that of the aluminum foam. As shown in Fig. 11, the decrement of the total heat transfer rate due to the dispersion of the Ag-MgO hybrid nanoparticles is more when ε is higher. A porous medium with a higher magnitude of porosity has more void spaces to be filled with the hybrid nanofluid. Hence, the increase of porosity boosts the effect of the presence of nanoparticles on the heat transfer. Based on Fig. 12, as γ increases, the Q_r of glass balls and aluminum foam augments and declines, respectively. When the solid matrix is made by glass balls, the magnitude order of the thermal conductivity of the solid matrix and the host fluid is the same. Hence, the variations of the γ parameter slightly affect the heat transfer rate.

Fig. 13 displays a comparison of the heat transfer rates of three different nanofluids containing the Ag-MgO hybrid nanoparticles, regular Ag, and MgO nanoparticles. The outcomes display that using all the mentioned nanoparticles declines the heat transfer rates. The decreasing functions of the heat transfer rates are linear for the regular Ag and MgO nanoparticles. Also, the reduction of the heat transfer rates due to dispersing Ag-MgO hybrid nanoparticles is much more than that of two other nanoparticles. The dynamic viscosity and thermal

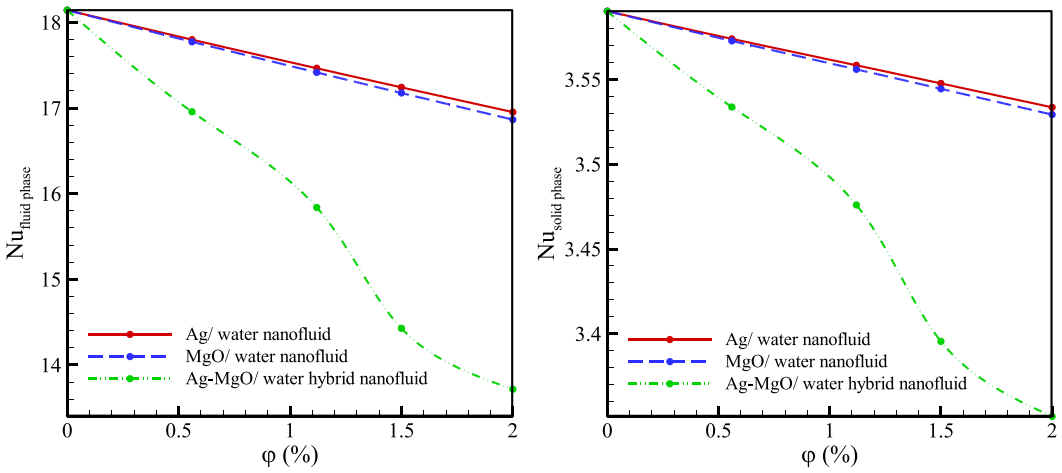

Fig. 13. Comparison between the average Nusselt numbers of Ag-MgO/ water hybrid nanofluid, Ag/ water, and regular MgO/ water nanofluids; $Ra = 1000$, $\varepsilon = 0.6$ and $H = \gamma = 10$.

conductivity presented in [59–61] are used for the regular nanofluids. Considering the variations of thermal conductivity and dynamic viscosity of the regular and hybrid nanofluid with the volume fraction, the non-linear behavior of the hybrid nanofluid, i.e., Ag-MgO/water, is dependent on the non-linear variations of the viscosity while varying the concentration as shown in Fig. 14.

5. Conclusion

Using LTNE model, the natural convection of Ag-MgO hybrid/water nanofluid flow through a porous enclosure has been studied. The Darcy model is utilized to analyze the flow dynamics through a porous material. The prevailing equations are transferred to dimensionless coordinates. Then, the Galerkin finite element method is applied to solve the equations. The non-uniform structured quadratic grid is employed to discretizing the physical domain. The summaries of the obtained results are listed below:

- An increment in *Ra* leads to a drastic augmentation in the vortex's strength. As *Ra* increases, the LTNE condition is amplified. Additionally, at low *Ra* values ($Ra = 10$ and 100), the influences of Ag-MgO hybrid nanoparticles on the thermal field of the solid phase are partly visible. Meanwhile, when $Ra = 1000$, the thermal field of the solid is not influenced by the Ag-MgO hybrid nanoparticles.
- Dispersing Ag-MgO hybrid nanoparticles leads to a reduction in the fluid flow strength and the heat transfer rate through the solid and fluid phases of the porous medium. Additionally, the use of hybrid nanoparticles weakens the LTNE condition.
- An increase of *H* causes the strength of vortices to enhance. As *H* increases, isotherms elongation of the fluid and solid phases decreases and increases, respectively. The impacts of dispersing the hybrid nanoparticles on the solid-phase temperature field are more significant when the *H* is high ($H = 100$ and 1000). Besides, as *H* increases, the effect of hybrid nanoparticles on the decrease of the local temperature difference of liquid and porous matrix reduces.
- This non-equilibrium is conducted to the thermal equilibrium state with the increase in γ. Also, the results indicate the heat transfer rates through the fluid and solid phases enhance with an increment in γ.
- The heat transfer rates through the nanofluid and solid matrix decline as the prosody, ε, increases. The decreasing rate of Nu_{hnf} with φ decline when ε rises. An opposite trend can be seen for the solid phase.
- The reduction of the heat transfer rates due to dispersing Ag-MgO hybrid nanoparticles is much more than that of Ag and MgO nanoparticles.
- When ε increases, the total heat transfer rate Q_{hnf} of glass balls and aluminum foam increases and decreases. It may also be observed that the total heat transfer ratio Q_r declines as ε augments.

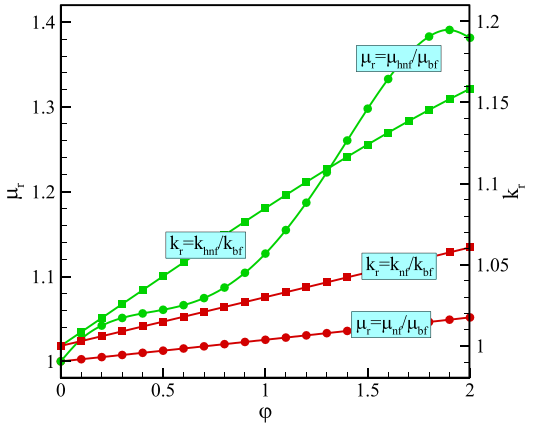

Fig. 14. Behaviors of the thermal conductivity and dynamic viscosity of the regular nanofluid (nf) and hybrid nanofluid (hnf) versus the volume fraction of nanoparticles.

In the present study, the flow and heat transfer of Ag and MgO hybrid nanofluids in a porous enclosure is addressed using the local thermal non-equilibrium model. The outcomes showed the significant influence of hybrid nanoparticles on the heat transfer behavior. Investigating the thermal performance of new types of hybrid nanoparticles and encapsulated phase change particles can be subject to future studies.

Declaration of Competing Interest

None.

References

[1] A. Amiri, K. Vafai, Transient analysis of incompressible flow through a packed bed, Int. J. Heat Mass Transf. 41 (1998) 4259–4279.
[2] K. Khanafer, K. Vafai, Isothermal surface production and regulation for high heat flux applications utilizing porous inserts, Int. J. Heat Mass Transf. 44 (2001) 2933–2947.
[3] K. Khanafer, K. Vafai, The role of porous media in biomedical engineering as related to magnetic resonance imaging and drug delivery, Heat Mass Transf. 42 (2006) 939.
[4] D.A. Nield, A. Bejan, Convection in Porous Media, Springer, 2006.

[5] K. Vafai, Porous Media: Applications in Biological Systems and Biotechnology, CRC Press, 2010.
[6] M. Izadi, N.M. Maleki, I. Pop, S. Mehryan, Natural convection of a hybrid nanofluid subjected to non-uniform magnetic field within porous medium including circular heater, Int. J. Numer. Methods Heat Fluid Flow 29 (4) (2019) 1211–1231.
[7] S. Mehryan, M. Izadi, Z. Namazian, A.J. Chamkha, Natural convection of multi-walled carbon nanotube–Fe_3O_4/water magnetic hybrid nanofluid flowing in porous medium considering the impacts of magnetic field-dependent viscosity, J. Therm. Anal. Calorim. 138 (2019) 1541–1555.
[8] M. Izadi, H.F. Oztop, M.A. Sheremet, S.A. Mehryan, N. Abu-Hamdeh, Coupled FHD–MHD free convection of a hybrid nanoliquid in an inversed T-shaped enclosure occupied by partitioned porous media, Numer. Heat Transf. A Appl. 76 (2019) 479–498.
[9] M. Izadi, S.A. Mohammadi, S. Mehryan, T. Yang, M.A. Sheremet, Thermogravitational convection of magnetic micropolar nanofluid with coupling between energy and angular momentum equations, Int. J. Heat Mass Transf. 145 (2019) 118748.
[10] A.J. Chamkha, H. Al-Naser, Double-diffusive convection in an inclined porous enclosure with opposing temperature and concentration gradients, Int. J. Therm. Sci. 40 (2001) 227–244.
[11] T. Basak, A.J. Chamkha, Heatline analysis on natural convection for nanofluids confined within square cavities with various thermal boundary conditions, Int. J. Heat Mass Transf. 55 (2012) 5526–5543.
[12] M. Ghalambaz, A.J. Chamkha, D. Wen, Natural convective flow and heat transfer of nano-encapsulated phase change materials (NEPCMs) in a cavity, Int. J. Heat Mass Transf. 138 (2019) 738–749.
[13] A. Hajjar, S.A.M. Mehryan, M. Ghalambaz, Time periodic natural convection heat transfer in a nano-encapsulated phase-change suspension, Int. J. Mech. Sci. 166 (2020) 105243.
[14] M. Sheikholeslami, CuO-water nanofluid free convection in a porous cavity considering Darcy law, Eur. Phys. J. Plus 132 (2017) 55.
[15] S.U.S. Choi, J.A. Eastman, Enhancing Thermal Conductivity of Fluids With Nanoparticles, 1995.
[16] C.-J. Ho, W.K. Liu, Y.S. Chang, C.C. Lin, Natural convection heat transfer of alumina-water nanofluid in vertical square enclosures: an experimental study, Int. J. Therm. Sci. 49 (2010) 1345–1353.
[17] Khalil Khanafer, Kambiz Vafai, Marilyn Lightstone, Buoyancy-driven heat transfer enhancement in a two-dimensional enclosure utilizing nanofluids, Int. J. Heat Mass Transf. 46 (2003) 3639–3653.
[18] J.M. Khodadadi, S.F. Hosseinizadeh, Nanoparticle-enhanced phase change materials (NEPCM) with great potential for improved thermal energy storage, Int. Comm. Heat Mass Transf. 34 (2007) 534–543.
[19] Apurba Kumar Santra, Swarnendu Sen, Niladri Chakraborty, Study of heat transfer augmentation in a differentially heated square cavity using copper–water nanofluid, Int. J. Therm. Sci. 47 (2008) 1113–1122.
[20] E. Abu-Nada, Z. Masoud, A. Hijazi, Natural convection heat transfer enhancement in horizontal concentric annuli using nanofluids, Int. Comm. Heat Mass Transf. 35 (2008) 657–665.
[21] M. Izadi, A. Behzadmehr, M.M. Shahmardan, Effects of inclination angle on mixed convection heat transfer of a nanofluid in a square cavity, Int. J. Comput. Methods Eng. Sci. Mech. 16 (2015) 11–21.
[22] M. Izadi, M.M. Shahmardan, M. Norouzi, A.M. Rashidi, A. Behzadmehr, Cooling performance of a nanofluid flow in a heat sink microchannel with axial conduction effect, Appl. Phys. A 117 (2014) 1821–1833.
[23] M.H. Esfe, H. Rostamian, M.R. Sarlak, M. Rejvani, A. Alirezaie, Rheological behavior characteristics of TiO2-MWCNT/10w40 hybrid nano-oil affected by temperature, concentration and shear rate: an experimental study and a neural network simulating, Physica E 94 (2017) 231–240.
[24] A. Fereidoon, S. Saedodin, M. Hemmat Esfe, M.J. Noroozi, Evaluation of mixed convection in inclined square lid-driven cavity filled with Al2O3/water nano-fluid, Eng. Appl. Comput. Fluid Mech. 7 (2013) 55–65.
[25] M.H. Esfe, S. Saedodin, M. Biglari, H. Rostamian, Experimental investigation of thermal conductivity of CNTs-Al2O3/water: a statistical approach, Int. Comm. Heat Mass Transf. 69 (2015) 29–33.
[26] M.H. Esfe, S. Saedodin, M. Biglari, H. Rostamian, An experimental study on thermophysical properties and heat transfer characteristics of low volume concentrations of Ag-water nanofluid, Int. Comm. Heat Mass Transf. 74 (2016) 91–97.
[27] M.H. Esfe, M.H. Hajmohammad, Thermal conductivity and viscosity optimization of nanodiamond-Co3O4/EG (40: 60) aqueous nanofluid using NSGA-II coupled with RSM, J. Mol. Liq. 238 (2017) 545–552.
[28] A. Alirezaie, S. Saedodin, M.H. Esfe, S.H. Rostamian, Investigation of rheological behavior of MWCNT (COOH-functionalized)/MgO-engine oil hybrid nanofluids and modelling the results with artificial neural networks, J. Mol. Liq. 241 (2017) 173–181.
[29] M.H. Esfe, H. Hajmohammad, R. Moradi, A.A.A. Arani, Multi-objective optimization of cost and thermal performance of double walled carbon nanotubes/water nanofluids by NSGA-II using response surface method, Appl. Therm. Eng. 112 (2017) 1648–1657.
[30] M.H. Esfe, K. Motahari, E. Sanatizadeh, M. Afrand, H. Rostamian, M.R.H. Ahangar, Estimation of thermal conductivity of CNTs-water in low temperature by artificial neural network and correlation, Int. Comm. Heat Mass Transf. 76 (2016) 376–381.
[31] M.H. Esfe, P. Razi, M.H. Hajmohammad, S.H. Rostamian, W.S. Sarsam, A.A.A. Arani, M. Dahari, Optimization, modeling and accurate prediction of thermal conductivity and dynamic viscosity of stabilized ethylene glycol and water mixture Al2O3 nanofluids by NSGA-II using ANN, Int. Comm. Heat Mass Transf. 82 (2017) 154–160.
[32] M.H. Esfe, P.M. Behbahani, A.A.A. Arani, M.R. Sarlak, Thermal conductivity enhancement of SiO 2–MWCNT (85: 15%)–EG hybrid nanofluids, J. Therm. Anal. Calorim. 128 (2017) 249–258.
[33] M.H. Esfe, S. Esfandeh, S. Saedodin, H. Rostamian, Experimental evaluation, sensitivity analyzation and ANN modeling of thermal conductivity of ZnO-MWCNT/EG-water hybrid nanofluid for engineering applications, Appl. Therm. Eng. 125 (2017) 673–685.
[34] M.H. Esfe, M. Rejvani, R. Karimpour, A.A.A. Arani, Estimation of thermal conductivity of ethylene glycol-based nanofluid with hybrid suspensions of SWCNT–Al 2 O 3 nanoparticles by correlation and ANN methods using experimental data, J. Therm. Anal. Calorim. 128 (2017) 1359–1371.
[35] S.H. Rostamian, M. Biglari, S. Saedodin, M.H. Esfe, An inspection of thermal conductivity of CuO-SWCNTs hybrid nanofluid versus temperature and concentration using experimental data, ANN modeling and new correlation, J. Mol. Liq. 231 (2017) 364–369.
[36] B. Ghasemi, S.M. Aminossadati, Brownian motion of nanoparticles in a triangular enclosure with natural convection, Int. J. Therm. Sci. 49 (2010) 931–940.
[37] Qiang Sun, Ioan Pop, Free convection in a triangle cavity filled with a porous medium saturated with nanofluids with flush mounted heater on the wall, Int. J. Therm. Sci. 50 (2011) 2141–2153.
[38] S.M. Aminossadati, B. Ghasemi, Enhanced natural convection in an isosceles triangular enclosure filled with a nanofluid, Comput. Math. Appl. 61 (2011) 1739–1753.
[39] J. Ali, Chamkha, Eiyad Abu-Nada, mixed convection flow in single- and double-lid driven square cavities filled with water–Al2O3 nanofluid: effect of viscosity models, Eur. J. Mech. B Fluids 36 (2012) 82–96.
[40] Omid Mahian, Lioua Kolsi, Mohammad Amani, Patrice Estellé, Goodarz Ahmadi, Clement Kleinstreuer, Jeffrey S. Marshall, Majid Siavashi, Robert A. Taylor, Hamid Niazmand, Somchai Wongwises, Tasawar Hayat, Arun Kolanjiyil, Alibakhsh Kasaeian, Ioan Pop, Recent advances in modeling and simulation of nanofluid flows-part I: fundamentals and theory, Phys. Rep. 790 (2019) 1–48.
[41] O. Mahian, L. Kolsi, M. Amani, P. Estellé, G. Ahmadi, C. Kleinstreuer, J.S. Marshall, R.A. Taylor, E. Abu-Nada, S. Rashidi, Recent advances in modeling and simulation of nanofluid flows-part II: applications, Phys. Rep. 790 (2019) 1–48.
[42] Jahar Sarkar, Pradyumna Ghosh, Arjumand Adil, A review on hybrid nanofluids: recent research, development and applications, Renew. Sust. Energ. Rev. 43 (2015) 164–177.
[43] M. Izadi, M.A. Sheremet, S. Mehryan, I. Pop, H.F. Öztop, N. Abu-Hamdeh, MHD thermogravitational convection and thermal radiation of a micropolar nanoliquid in a porous chamber, Int. Comm. Heat Mass Transf. 110 (2020) 104409.
[44] M. Izadi, G. Hoghoughi, R. Mohebbi, M. Sheremet, Nanoparticle migration and natural convection heat transfer of Cu-water nanofluid inside a porous undulant-wall enclosure using LTNE and two-phase model, J. Mol. Liq. 261 (2018) 357–372.
[45] M. Izadi, R. Mohebbi, A.A. Delouei, H. Sajjadi, Natural convection of a magnetizable hybrid nanofluid inside a porous enclosure subjected to two variable magnetic fields, Int. J. Mech. Sci. 151 (2019) 154–169.
[46] M. Izadi, S. Sinaei, S. Mehryan, H.F. Oztop, N. Abu-Hamdeh, Natural convection of a nanofluid between two eccentric cylinders saturated by porous material: Buongiorno's two phase model, Int. J. Heat Mass Transf. 127 (2018) 67–75.
[47] Ammar I. Alsabery, Rasul Mohebbi, Ali J. Chamkha, Ishak Hashim, Effect of local thermal non-equilibrium model on natural convection in a nanofluid-filled wavy-walled porous cavity containing inner solid cylinder, Chem. Eng. Sci. 201 (2019) 247–263.
[48] M. Izadi, R. Mohebbi, H. Sajjadi, A.A. Delouei, LTNE modeling of magneto-Ferro natural convection inside a porous enclosure exposed to nonuniform magnetic field, Physica A 535 (2019) 122394.
[49] M. Izadi, S. Mehryan, M.A. Sheremet, Natural convection of CuO-water micropolar nanofluids inside a porous enclosure using local thermal non-equilibrium condition, J. Taiwan Inst. Chem. Eng. 88 (2018) 89–103.
[50] S. Mehryan, M. Ghalambaz, M. Izadi, Conjugate natural convection of nanofluids inside an enclosure filled by three layers of solid, porous medium and free nanofluid using Buongiorno's and local thermal non-equilibrium models, J. Therm. Anal. Calorim. 135 (2019) 1047–1067.
[51] S. Mehryan, M. Izadi, M.A. Sheremet, Analysis of conjugate natural convection within a porous square enclosure occupied with micropolar nanofluid using local thermal non-equilibrium model, J. Mol. Liq. 250 (2018) 353–368.
[52] S. Sivasankaran, A.I. Alsabery, I. Hashim, Internal heat generation effect on transient natural convection in a nanofluid-saturated local thermal non-equilibrium porous inclined cavity, Physica A 509 (2018) 275–293.
[53] M. Ghalambaz, M.A. Sheremet, S.A. Mehryan, F.M. Kashkooli, I. Pop, Local thermal non-equilibrium analysis of conjugate free convection within a porous enclosure occupied with Ag–MgO hybrid nanofluid, J. Therm. Anal. Calorim. 135 (2019) 1381–1398.
[54] Mohammad Hemmat Esfe, Ali Akbar Abbasian Arani, Mohammad Rezaie, Wei-Mon Yan, Arash Karimipour, Experimental determination of thermal conductivity and dynamic viscosity of Ag–MgO/water hybrid nanofluid, Int. Comm. Heat Mass Transf. 66 (2015) 189–195.
[55] K. Rajesh Nimmagadda, Venkatasubbaiah, conjugate heat transfer analysis of microchannel using novel hybrid nanofluids (Al2O3+Ag/Water), Eur. J. Mech. B Fluids 52 (2015) 19–27.
[56] J. Donea, A. Huerta, Finite Element Methods for Flow Problems, John Wiley & Sons, 2003.

[57] M.A. Sheremet, T. Grosan, I. Pop, Free convection in a square cavity filled with a porous medium saturated by nanofluid using Tiwari and Das' nanofluid model, Transp. Porous Media 106 (2015) 595–610.
[58] A. Cihat Baytas, Ioan Pop, free convection in a square porous cavity using a thermal nonequilibrium model, Int. J. Therm. Sci. 41 (2002) 861–870.
[59] Heidar Hashemi, Zafar Namazian, S.A.M. Mehryan, Cu-water micropolar nanofluid natural convection within a porous enclosure with heat generation, J. Mol. Liq. 236 (2017) 48–60.
[60] A.J. Chamkha, Am Rashad, M.A. Mansour, T. Armaghani, M. Ghalambaz, Effects of heat sink and source and entropy generation on MHD mixed convection of a Cu-water nanofluid in a lid-driven square porous enclosure with partial slip, Phys. Fluids 29 (2017) 52001.
[61] M. Sabour, M. Ghalambaz, A. Chamkha, Natural convection of nanofluids in a cavity: criteria for enhancement of nanofluids, Int. J. Numer. Methods Heat Fluid Flow 27 (2017) 1504–1534.